Journal of Hydrology 592 (2021) 125763

Contents lists available at ScienceDirect

Journal of Hydrology

journal homepage: www.elsevier.com/locate/jhydrol

Research paper

Modelling the sources and transport of ammonium nitrogen with the SPARROW model: A case study in a karst basin

Yibin Dai [a], Yunchao Lang [a,b,*], Tiejun Wang [a,b,*], Xiaokun Han [a,b], Lichun Wang [a,b], Jun Zhong [a,b]

[a] Institute of Surface-Earth System Science, School of Earth System Science, Tianjin University, Weijin Road 92, Tianjin 300072, PR China
[b] Tianjin Key Laboratory of Earth Critical Zone Science and Sustainable Development in Bohai Rim, Tianjin University, Weijin Road 92, Tianjin 300072, PR China

ARTICLE INFO

Keywords:
Water quality
Karst
The SPARROW model
Ammonium nitrogen
The Wujiang River Basin

ABSTRACT

The assessment of nutrients delivered to aquatic ecosystems is important for water quality controls. Mainly due to the complex terrains and subsurface hydrological systems in karst regions, it is challenging to understand nutrient delivery pathways and quantify contributions of various sources to surface waterbodies in karst basins, e.g., via the use of mechanistic models. To resolve this issue, a statistical water quality model (i.e., the SPAtially Referenced Regression On Watershed attributes-SPARROW model) was tested to estimate the mean annual transport, concentration, and yield of ammonium nitrogen (NH_4^+-N) contributed by natural and human sources in the Wujiang River Basin (WRB) in southwest China, where the nutrient inputs and pathways have been significantly altered by anthropogenic activities. Overall, the modelling results explained about 86% of the variability in the observed mean annual NH_4^+-N fluxes, attesting the applicability of the SPARROW model for estimating NH_4^+-N transport at mean annual time scales in karst basins. Moreover, the results indicated that the anthropogenic sources (i.e., fertilizer, livestock manure, and waste water) were the main origins of NH_4^+-N, accounting for a total load of 66.8% in waterbodies. In addition, the leakage of NH_4^+-N into groundwater from the karst area was evaluated, leading to a reduction of NH_4^+-N delivery to surface waterbodies for about 36.9% with a range from 31.3% to 52.2% in the seven main subbasins in the WRB. The damming effect of the constructed reservoirs on the NH_4^+-N delivery differed noticeably with the lowest reduction rate (2.4%) in the Suofengying reservoir and the highest rate (79.1%) in the Hongfenghu reservoir. It was found that the interception efficiency of lake-type reservoirs was generally higher than that of river-type reservoirs in the WRB. The results of this study demonstrate the usefulness of the SPARROW model for evaluating nutrient transport and pathways in karst regions, which can provide critical information for better management to control nutrients in those regions.

1. Introduction

Nutrient availability is one of the key factors for controlling water quality in aquatic ecosystems. Excessive nutrients in aquatic systems can affect ecosystem integrity, human health, drinking water supplies, and local amenities (Abbaspour et al., 2007; Perrin et al., 2014). Therefore, it is important to understand the pathways, through which nutrients of various natural and anthropogenic sources enter aquatic ecosystems. Although numerous studies have showed the impacts of environmental factors, such as climate, topography, soil, and vegetation, on nutrient transport pathways (Kyllmar et al., 2006; Qin et al., 2010), it is still a grand challenge to reliably estimate nutrient transport in large basins with complex river networks, which is further complicated by variations in landscapes and removal processes (Chen et al., 2019).

Karst regions are of hydrological, ecological, and socioeconomic significance with unique topography and subsurface structures (Han et al., 2014; Jiang et al., 2014), which cover ~10% of the Earth surface and provide drinking water to ~25% of the world population (Kalhor et al., 2019). However, intensive human activities in those regions, such as agriculture and urbanization, have significantly changed the nutrient inputs and pathways from natural conditions (Li et al., 2020). Moreover, with the demands for water resources allocation and flood control, a large portion of rivers in karst regions in southwest China have been impounded and their hydrological continuity has been altered (Li et al.,

* Corresponding authors at: Institute of Surface-Earth System Science, School of Earth System Science, Tianjin University, Weijin Road 92, Tianjin 300072, PR China.

E-mail addresses: yunchao.lang@tju.edu.cn (Y. Lang), tiejun.wang@tju.edu.cn (T. Wang).

https://doi.org/10.1016/j.jhydrol.2020.125763
Received 13 October 2020; Received in revised form 6 November 2020; Accepted 9 November 2020
Available online 18 November 2020
0022-1694/

2016). The dams can affect local biogeochemical cycles in many different ways. For example, numerous studies focused on the interception effect of reservoirs on nutrient transport (Seitzinger et al., 2002; Wang et al., 2010), as the interception by dams can considerably reduce the delivery flux and promote the accumulation of nutrients in reservoirs (Harrison et al., 2009). These changes can further break the balance of local ecosystems; for instance, the excess nutrients might increase the risk of algal bloom and deteriorate aquatic habitats (W. Wang et al., 2019).

Process-based mechanistic models have been widely used in evaluating nutrient transport in non-karst basins, which vary considerably in model structures and governing equations used to depict the pathways and interactions of nutrients with surrounding environments (Singh et al., 2005; Hashemi et al., 2016). However, intensive data requirements of process-based models (e.g., land use types, soil parameters; Čerkasova et al., 2018) for simulating nutrient transport generally limit the application of those models in karst basins, primarily owing to their complex subsurface systems that are composed of karst fissures, pipelines, and caves (Jiang et al., 2014). These subsurface features can promote the leakage of surface water to groundwater, and thus exert significant impacts on nutrient transport (Tooth and Fairchild, 2003; Song et al., 2019). Therefore, the development of suitable models other than process-based models for karst regions has attracted much attention in scientific communities over the past several decades (Hartmann et al., 2014; Amin et al., 2016).

Ammonium nitrogen (NH_4^+-N) is an important nutrient that commonly exists in products from human activities like fertilizer, livestock excrement, and waste water. Most NH_4^+-N is fixed through microorganisms and the Haber-Bosch process, of which 80% is used as agricultural fertilizer and 20% as feedstock for industrial processes (Fowler et al., 2013). Additionally, NH_4^+-N can be decomposed from organic matter through ammonification. With high activities, NH_4^+-N can be transformed to nitrite (NO_2^-) and nitrate (NO_3^-) nitrogen through nitrification, and to nitrogen (N_2) through anammox reactions, or be assimilated and converted to organic nitrogen by plants and bacteria (Xia et al., 2018). As NH_4^+-N can tremendously affect local water quality (Peterson et al., 2001), it is of great importance to estimate the sources and transport pathways of NH_4^+-N for water quality management. However, as mentioned before, it is extremely difficult for process-based models to simulate the transport of NH_4^+-N at regional scales in karst regions, with limited observational data and high uncertainties in model parameterizations (Malagò et al., 2016; Hartmann et al., 2014). To this end, statistic models may provide alternatives for assessing nutrient transport in karst regions, as they allow extracting information from available data with minimum assumptions and thus are more appropriate for hydrological systems with unknown nutrient flow pathways (Li et al., 2015).

Here, the SPAtially Referenced Regression On Watershed attributes (SPARROW) model was used in this study, which is a statistical water quality model designed for basin-scale studies on nutrient transport (Smith et al., 1997). The SPARROW model integrates the information on nutrient sources and landscape properties to quantify nutrient transport. The model has been extensively used in non-karst regions in Canada, China, Japan, New Zealand, Spain, and the U.S. with satisfactory performance results (Smith et al., 1997; Alexander et al., 2002, 2007; Aguilera et al., 2012; Wellen et al., 2012; Duan et al., 2015; Li et al., 2015). Furthermore, the model performed well in assessing nutrient transport in large-scale reservoirs (Brown et al., 2011; Morales-Marín et al., 2017) as well as in simulating scenarios with changing nutrient sources or landscape conditions (Garcia et al., 2011; Alshawaf et al., 2016). In spite of its wide applications, the applicability of the SPARROW model in karst regions has not been tested, which might provide an additional avenue for modelling nutrient transport in karst regions with complex terrains and subsurface systems.

As the first attempt, the main objectives of this study were to (1) test the applicability of the SPARROW model in karst regions and (2) quantify the NH_4^+-N sources via natural and anthropogenic inputs and assess their transport processes affected by various natural and anthropogenic factors (particularly, the impacts of karst geology and reservoirs on the regional NH_4^+-N transport). To this end, the Wujiang River Basin (WRB), a large karst basin located in southwest China was selected, where the nutrient inputs and pathways have been significantly altered by anthropogenic activities in recent years. Based on the model results, an assessment for different management strategies was also made. It was expected that the SPARROW model could assist with policy decision support for better management in controlling NH_4^+-N in karst regions.

2. Data and methodology

2.1. Study area

The WRB is located in Guizhou province in southwest China (Fig. 1). It is the one of the largest tributaries in the Yangtze River basin, with a drainage area of 66,807 km^2. The WRB lies in a subtropical monsoon climate zone with a mean annual temperature of 12.3 °C, where the respective highest and lowest temperature is in July (26 °C on average) and January (3.5 °C). The mean annual precipitation (P) is around 1000 mm with ~75% of P occurring in summer months. The main land use types in the WRB are cultivated land, grass land, and forest land. Due to the mountainous terrains, the cultivated lands are mainly distributed in topographic depressions and valleys, while grass lands are scattered along hillsides for grazing. The forests are dominated by coniferous and deciduous trees (Han et al., 2014). The urban population in Guizhou province is only about 35% of the total population with the population density decreasing from southwest to northeast.

About 70% of the WRB belongs to karst landscapes (Fig. 2), which are characterized by thin soil layers underlain by carbonate rocks and complicated groundwater systems. In the past several decades, intensive human activities (e.g., deforestation and overgrazing) have led to significant soil erosion and rock desertification, which subsequently caused serious environmental hazards such as landslides and floods (Yuan, 1997). The rock desertification in the karst area has been recognized as a major hindrance for local agricultural development (Li et al., 2020), and also poses tremendous effects on hydrologic processes, particularly on runoff generation processes. For instance, the loss of soil and vegetation in karst fractures increased the water leakage to groundwater systems and decreased the resistance to overland flow in areas with high relief (Jiang et al., 2014).

There are seven main subbasins in the WRB according to the tributary areas (Fig. 1), including the Sancha River (SCR), the Liuchong River (LCR), the Yachi River (YCR), the Maotiao River (MTR), the Qingshui River (QSR), the Xiang River (XR), and the Wujiang Mainstream (WJM) subbasins. The SCR and LCR subbasins represent the upstream area, the YCR, MTR, QSR and XR subbasins represent the midstream area, and the WJM subbasin belongs to the downstream area. The main stream has a mean annual water discharge of 5.34×10^{10} m^3, which accounts for approximately 47% of the total surface water runoff in Guizhou Province (Huang et al., 2017). The abundant waterflow and large altitude drop make the WRB ideal for exploiting hydropower, which led to the construction of several large-scale reservoirs along the rivers in the WRB (Liu et al., 2011; B. Wang et al., 2019). These reservoirs are for multiple purposes, including hydropower generation, agricultural irrigation, human and animal water consumption, and flood risk management (Feng et al., 2009).

2.2. Description of the SPARROW model

The statistical SPARROW model was developed by the USGS, which combines water quality observations with landscape and nutrient information to estimate annual-averaged nutrient loads exported from land surface to waterbodies. This model requires less data than numerical mechanistic models, and also overcomes the shortcomings of

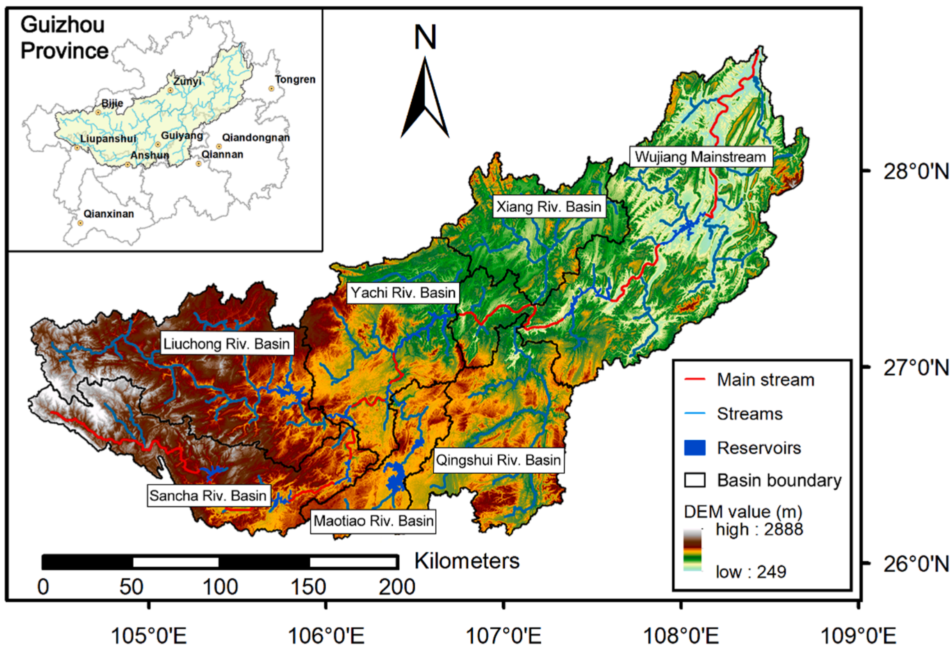

Fig. 1. Geographical location, streams, reservoirs, digital elevation model (DEM) and seven main subbasin areas of the WRB.

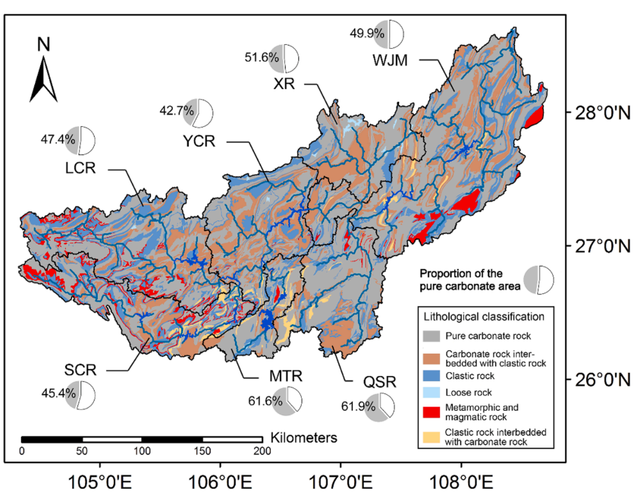

Fig. 2. The lithological map of the WRB and the proportion of pure carbonate area in seven main subbasins.

traditional regression-based statistical models by including mass-balance constrained components (e.g., flow pathways and decay processes), non-linear interactions of nutrients with landscapes, and spatially distributed basin attributes (Alexander et al., 2000, 2002). The model is generally applied in large-scale basins due to the use of statistic approaches in the model. It performs well in identifying nutrient sources, analyzing environmental factors, and evaluating water quality (Schwarz et al., 2006).

To be self-contained, a brief description of the SPARROW model is provided here, and the detailed information can be found elsewhere in the literature (Schwarz et al., 2006). The estimated load of nutrients is computed by the following equation:

$$F_i^*=\underbrace{\left[\sum_{j\in J(i)} F_j^{'}\right]\delta_i A\left(Z_i^S, Z_i^R;\theta_S,\theta_R\right)}_{A}+\underbrace{\left[\sum_{n=1}^{N_S} S_{n,i}\,\alpha_n D_n\left(Z_i^D;\theta_D\right)\right]A^{'}\left(Z_i^S,\ Z_i^R;\theta_S,\theta_R\right)}_{B} \quad (1)$$

where F_i* represents the estimated load leaving the reach i. The first term A at the right side of Eq. (1) is the amount of flux that is delivered to the downstream reach i from the adjacent upstream reach j. If measured data are available in the upstream reach j, $F_j^{'}$ is set to be equal to measured fluxes as F_j^M; otherwise, $F_j^{'}$ is given by estimated fluxes in the model. The parameter δ_i is the fraction of the upstream flux delivered to reach i and set to 1 if there are no diversions.

The lumped term $A(Z_i^S, Z_i^R;\theta_S,\theta_R)$ is the delivery function for streams and reservoirs, representing attenuation processes along the water pathway (the same for $A'(Z_i^S, Z_i^R;\theta_S,\theta_R)$ in the term B). This function defines the fraction of the flux in reach i that is delivered to the downstream node (i.e., $i+1$) by the following two equations based on the reach types (i.e., stream or reservoir):

$$A\left(Z_i^S;\theta_S\right) = exp\left(-\sum_{c=1}^{C_S}\theta_{Sc}T_{c,i}^S\right) \quad (2)$$

$$A\left(Z_i^R;\theta_R\right) = \frac{1}{1+\theta_R\left(q_i^R\right)^{-1}} \quad (3)$$

The factor $A(\cdot)$ is a function of stream or reservoir characteristics, denoted by the vectors Z_i^S (i.e., $T_{c,\ i}^S$, in this study, represents the mean travel time as the quotient of the stream length to the mean velocity of the flow along the water pathway) and Z_i^R (i.e., q_i^R, in this study, represents the areal hydraulic load as the quotient of the outflow discharge to the water area of the reservoir), with θ_S and θ_R being the corresponding coefficient vectors. The notation C_S in Eq. (2) is the number of stream classes defined by the intervals of mean streamflow.

The second lumped term B is the amount of the flux that is originated from the subbasin i directly transported to reach i. The parameter $S_{n,\ i}$ is the source n in the subbasin i contributed to reach i with the corresponding coefficient α_n. The term $D_n(Z_i^D;\theta_D)$ represents the net impact of the environment factor Z_i^D on nutrient transport in subbasin i, with the corresponding coefficient θ_D described by the following equation:

$$D_n\left(Z_i^D;\theta_D\right) = exp\left(\sum_{m=1}^{M_D} \omega_{nm} Z_{m\ i}^D \theta_{Dm}\right) \quad (4)$$

The notation M_D is the number of environment factors, and ω_{nm} is an indicator with a value of 1 or 0 for whether the environment factor *m* affects source *n*. All the coefficients in the above equations are calibrated by a non-linear least square method between the observation and prediction. In this study, the model performance was evaluated by several indexes: the significance level of the variables (*p*-value), the coefficient of determination (R^2), root mean square error (RMSE; the error in model predictions), the spatial distribution of residuals (the difference between prediction and observation), and robustness of coefficients (bootstrap estimation).

2.3. Data preparation

In order to run the SPARROW model for the time period from 2010 to 2012, several types of data were required, including hydrological stream networks, water quality and flow rate records, nutrient exports from different sources, and environment settings of the basin (Schwarz et al., 2006).

2.3.1. Stream network and flow data

In this study, a digital elevation model (DEM) of a spatial resolution of 30 m from the Geospatial Data Cloud site (http://www.gscloud.cn) was used to derive the stream network in the WRB using ArcGIS version 10.2 (see the Supplementary materials). There were 220 reaches delineated in the WRB with 12 reservoirs (Fig. 3). Due to the lack of flow data at some reaches, the annual streamflow rates at those reaches were estimated by the Budyko model (Zhang et al., 2004) through annual *P* and potential evapotranspiration (E_0) in the following equation:

$$Q = \left(P^{\frac{1}{1-\alpha}} + E_0^{\frac{1}{1-\alpha}}\right)^{1-\alpha} - E_0 \quad (5)$$

The annual *P* data were obtained from the Resource and Environment Data Cloud Platform (REDCP, http://www.resdc.cn/) and the annual E_0 data were retrieved from the Modis16A3 dataset (https://lpdaac.usgs.gov/). The parameter α in Eq. (5) was calibrated at 30 hydrological stations in the WRB with flow records from 2010 to 2012 (Fig. 4). Then, the model was applied to predict the annual streamflow rates of unmonitored reaches, which was then combined with the Manning equation to estimate the mean flow velocity based on statistical approaches (Schulze et al., 2005).

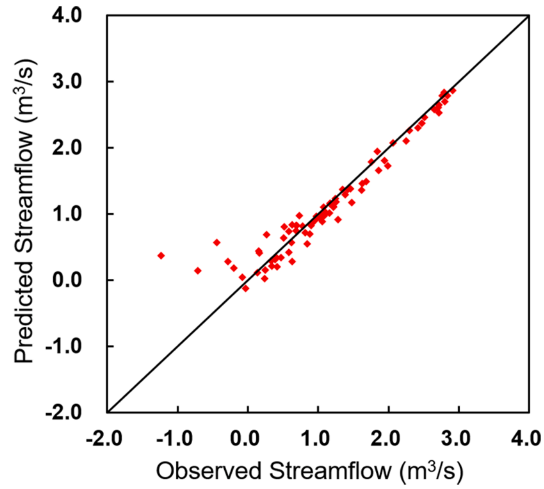

Fig. 4. Logarithm-transformed predicted vs observed streamflow.

2.3.2. NH_4^+-N load flux

There were 16 monitoring stations with monthly NH_4^+-N concentration data and 13 stations with yearly-averaged NH_4^+-N concentration data during 2010–2012 from the Hydrology and Water Resources Bureau of Guizhou Province. The mean annual load of 2010 to 2012 was estimated by the following equation:

$$\text{Load} = C_i \cdot Q_i \quad (6)$$

The C_i represents the mean annual concentration of NH_4^+-N at 29 sites and the Q_i is the mean annual streamflow rate computed in Section 2.3.1 (see Fig. S1 for the comparison of monthly-based and yearly-based mean annual load estimation in the Supplementary materials). The loads of NH_4^+-N were used for the model calibration.

2.3.3. NH_4^+-N sources

The NH_4^+-N in the WRB was mostly from fertilizer, livestock manure, waste water, and natural organic matter (Li et al., 2013; Li and Ji, 2016). The mostly used nitrogen fertilizer in the WRB was urea, which contains two amino groups in one molecule ($(NH_2)_2CO$). The NH_4^+-N input from the fertilizer application to the land surface was estimated from the

Information of 12 reservoirs in WRB.

No.	Reservoir Name	Surface Area [a] (km^2)
1	Hongjiadu (HJD)	41.85
2	Pingzhai (PZ)	12.74
3	Puding (PD)	11.24
4	Yinzidu (YZD)	7.70
5	Dongfeng (DF)	9.81
6	Hongfenghu (HFH)	44.78
7	Baihuahu (BHH)	9.91
8	Hongyan (HY)	1.20
9	Suofengying (SFY)	3.10
10	Wujiangdu (WJD)	40.35
11	Goupitan (GPT)	31.31
12	Silin (SL)	24.30

[a] The impoundment surface area was extracted from satellite images.

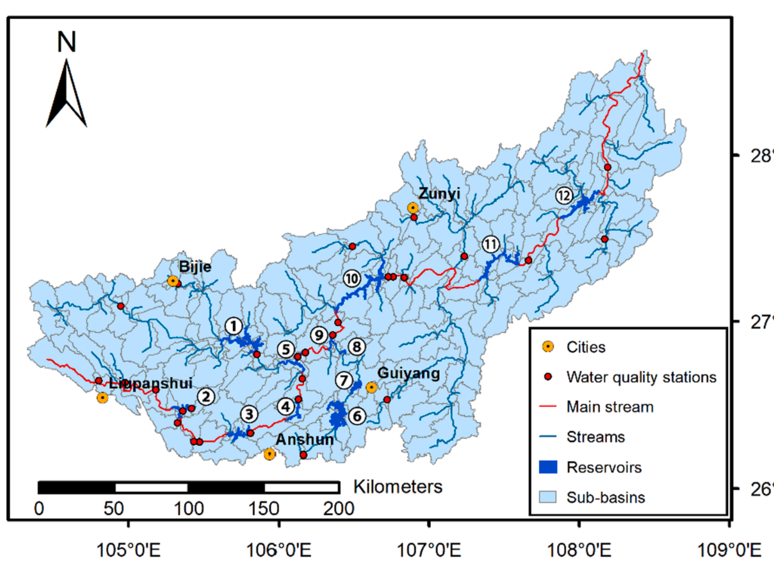

Fig. 3. Stream network of the WRB. The location of the main cities and water quality stations are labeled in the map. The information of the 12 reservoirs is listed in the table.

county-based yearbook around 2010, while the NH_4^+-N input from livestock manures to the land surface was estimated from the dataset of the First China Pollution Census. The atmospheric deposition of NH_4^+-N was neglected in this study, as the simulation results in L. Zhang et al. (2018) indicated that the NH_4^+-N deposition in the WRB was ~4 kg ha^{-1} $year^{-1}$, which was much less than the loads from fertilizer (~36 kg ha^{-1} $year^{-1}$) and manure (~25 kg ha^{-1} $year^{-1}$). The land use types (i.e., cultivated land, grass land, and forest land data were obtained from the REDCP) were used as surrogates for non-point sources (i.e., the NH_4^+-N from agriculture, grazing, and nature, respectively). Additionally, the population data from the REDCP were used as the surrogate for anthropogenic NH_4^+-N sources, for example, the loads from sewage/industrial waste water. All the above-mentioned data were compiled for the 220 subbasins in the Supplementary materials (Figs. S2–S8).

2.3.4. Land-to-water delivery factors

To consider the impacts of environmental factors on the delivery of NH_4^+-N from land to waterbodies, several variables of climate and landscape were included in this study. These variables have been widely recognized as important factors for controlling the transport of nutrients. For example, *P* could promote the delivery of nutrients through runoff generation (Morales-Marín et al., 2017), while high soil permeability could promote infiltration and remove nutrients from soil (Robertson and Saad, 2011). Specifically, *P*, air temperature, and soil texture datasets were compiled from the REDCP. The stream density and slope datasets were extracted from the DEM data. The soil permeability was estimated from the ROSSETA model according to the soil texture (Y. Zhang et al., 2018). To examine the karstification impact on the NH_4^+-N transport, the carbonate rock distribution was extracted from the hydrogeological map from the Institute of Karst Geology, Chinese Academy of Geological Sciences (http://www.karst.cgs.gov.cn/). These variables were allocated to the 220 subbasins (Figs. S9–S14 in the Supplementary materials), and then input and tested in the model.

The typical karst characteristics of fissure and pipeline are mainly developed in the pure carbonate area, and the corresponding storage capacity could increase the transit times (Lauber and Goldscheider, 2014; Zhang et al., 2020a). In addition, several studies have found that there was a large amount of surface nutrients leaked to groundwater in karst regions under laboratory or field conditions (Wei et al., 2011; Peng et al., 2019). Therefore, the leaked NH_4^+-N in carbonate aquifers could be stored and converted to other nitrogen forms (e.g., to NO_3^--N through nitrification and/or N_2 through anammox) before being delivered to surface waters (Zhang et al., 2020b). However, with the complex terrains and subsurface structures, it was hard to obtain detailed hydrogeological data in the WRB region. Thus, the distribution of the pure carbonate area (Fig. 2) was used to represent the net effect from karstification on the NH_4^+-N transport.

2.4. Model setup and calibration

The SPARROW model parameters were calibrated through a nonlinear least square regression method (Schwarz et al., 2006). Different combinations of NH_4^+-N sources and environmental factors were tested based on the assessment indexes used in this study (e.g., *p*-value and R^2), and the best specification was chosen for the WRB. In this study, 8 variables were selected from the 16 variables listed in Table 1.

For NH_4^+-N sources, the population and forest land were chosen to represent anthropogenic (e.g., fertilizer, manure waste, sewage, and industrial water) and natural (e.g., NH_4^+-N decomposed from organic matter in soil and defoliation) sources, respectively (see correlation analysis in the Supplementary materials). The climate in the WRB is of a sub-humid type with mean annual *P* ranging roughly from 800 mm/year to 1200 mm/year. The abundant *P* leads to large surface runoff and infiltration, thus delivering a significant amount of NH_4^+-N into adjacent waterbodies and groundwater. In addition, a significant portion of the WRB is covered by carbonate rocks. With the high solubility of carbonate rocks, there are generally well-developed groundwater systems underlain the carbonate areas, which may have a profound impact on the transport of NH_4^+-N. For the NH_4^+-N decay processes in waterbodies, the model took the characteristics of stream and reservoir into consideration.

Table 1
The input variables in the SPARROW model.

Parameter	Name	Model Input	Unit
Sources	Fertilizer		kg/year
	Manure		kg/year
	Cultivated land		km^2
	Grass land		km^2
	Population	√	person
	Forest land	√	km^2
Environmental factors	Precipitation	√	cm
	Carbonate area	√	km^2
	Temperature		°C
	Drainage density		km/km^2
	Slope		%
	Permeability		cm/h
Water attributions	Stream velocity	√	m/s
	Stream length	√	km
	Reservoir water area	√	km^2
	Reservoir discharge	√	m^3/s
Number	16	8	

In order to quantify the theoretical maximum reduction in the NH_4^+-N transport associated with the carbonate area, the predicted load was compared with a hypothetical scenario without the impact of the carbonate area. Therefore, the difference between these two scenarios could indicate the reduction proportion of NH_4^+-N by the leakage effect due to carbonate rocks. It should be noted that the estimation was based on the simplification that possible changes associated with the carbonate area were not considered in the hypothetical scenario (i.e., the simulated processes such as runoff generation might be changed when the carbonate area was excluded).

As for the evaluation of the NH_4^+-N loads intercepted by the reservoir, the difference between the input and output loads of the reservoir was estimated based on the model simulation. The input loads into the reservoir were the sum of the loads from upstream (external sources) and adjacent areas (internal sources). The output loads were that delivered to the adjacent downstream reach of the reservoir. The interception efficiency was then defined as the quotient of interception loads to input loads.

3. Results and discussion

3.1. Model evaluation

The simulation results from the SPARROW model in the WRB explained about 86% of the variability in the log-transformed (i.e., for better illustration of the values in different orders of magnitude) mean annual NH_4^+-N loads (Fig. 5a). The RMSE value of the model results (0.74) and the bootstrap coefficients of variables also showed good robustness of the model (Table 2). The *p*-values for the source variables (e.g., population and carbonate area) were <0.05. The decay of NH_4^+-N in streams showed a *p* value of 0.053, while the variables of *P*, forest land, and reservoir decay did not show good correlations. Note that except for the significance level, the interpretability of model results is another important metric for assessing model performances (Zhou et al., 2018). In this study, the population distribution and forest land represented the NH_4^+-N from anthropogenic and natural sources, respectively. With the low surface runoff coefficient and widely distributed carbonate areas in karst regions, *P* tended to promote surface NH_4^+-N infiltration into groundwater (Peng et al., 2019), and the long transit times could promote NH_4^+-N in carbonate aquifers to be stored and converted to other nitrogen forms (Zhang et al., 2020b); whereas, biogeochemical

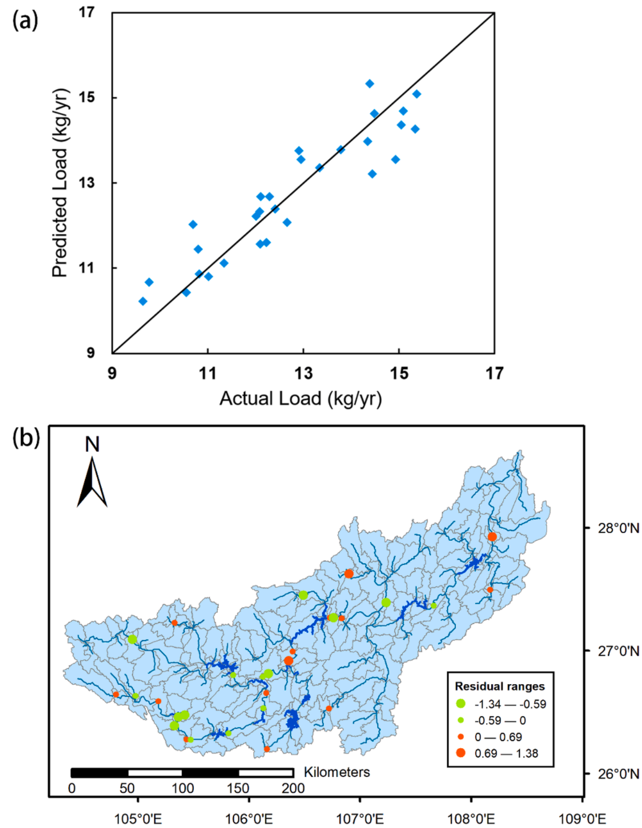

Fig. 5. (a) Logarithm-transformed predicted vs observed NH_4^+-N load at monitoring stations and (b) the map of logarithm-transformed residual in the basin.

processes (e.g., nitrification, assimilation, and deposition) in streams and reservoirs were related to decay processes in the model (i.e., the instream loss in Table 2 was depicted by stream velocity and length in Eq. (2), and the reservoir attenuation was depicted by water area and discharge in Eq. (3)). These variables were all physically important for interpreting the transport of NH_4^+-N. Several reasons might lead to the insignificance of the variables, such as insufficient observations for model calibrations, spatial heterogeneities of model variables, and uncertainties of measured data (Schwarz et al., 2006).

The spatial distribution of the log-transformed residuals is presented in Fig. 5b, which provides information as to whether the model overestimated or underestimated NH_4^+-N loads compared to observations. Fig. 5b indicates that the model tended to underestimate the load for headwaters, likely due to the uncertainties in predicted streamflow in headwaters (i.e., the comparatively larger deviation for low streamflow in Fig. 4). Overall, the positive and negative residuals were uniformly distributed across the WRB rather than centered in a particular area, suggesting that the model had been adequately specified (McMahon et al., 2003).

3.2. Source contribution, load flux, and concentration prediction for NH_4^+-N

The model estimated the contributions of NH_4^+-N loads into waterbodies from both anthropogenic and natural sources for the 220 subbasins in the WRB, with the respective average contribution of 66.8% and 33.2%. The source contributions for the seven main subbasins are presented in Fig. 6a, which shows that NH_4^+-N was mainly derived from anthropogenic sources in the upstream and midstream subbasins (>70%). These subbasins cover most of the urban areas in the WRB, where industrial and municipal sewage provided large quantities of NH_4^+-N. In addition, the percentage of cultivated and grass lands was also relatively high in the upstream and midstream areas, leading to intensive fertilizer use and manure from grazing. In contrast, forest lands were centered in the downstream area (i.e., WJM), where the contributions of NH_4^+-N from natural and anthropogenic sources were approximately equal. Another reason for the relatively lower anthropogenic contribution in the WJM was the lack of large cities, which gave little industrial or sewage wastewater to waterbodies.

The three-year-averaged NH_4^+-N loads (i.e., 2010–2012) through the 220 reaches are displayed in Fig. 6b. The load from each reach was contributed by local and adjacent upstream sources. With the accumulation of NH_4^+-N along the stream, higher loads were expected in the downstream area. Moreover, among the 12 reservoirs located along the tributaries and main stream, the interception efficiency of NH_4^+-N varied noticeably (more discussion in Section 3.3). The decay processes of NH_4^+-N in streams might be owing to the algae absorption and nitrification (Wang et al., 2002). By comparison, the decreased delivery flux in reaches closer to the basin outlet could be owing to less loads delivered from tributaries nearby. Since the SPARROW model was implemented with first-order decay rates in streams (i.e., the decay rate is proportional to the NH_4^+-N flux), the amount of NH_4^+-N that decayed in downstream reaches (with higher NH_4^+-N fluxes) was larger and the reduction in NH_4^+-N fluxes was thus more pronounced. For reaches adjacent to urban areas (especially to the cities of Guiyang and Zunyi), higher loads might be owing to the large amount of industrial and

Table 2
The SPARROW model coefficients calibrated by 29 observations in WRB.

Parameter	Calibration model coefficient	Probability level (*p*-value)	Standard error of coefficient	Nonparametric bootstrap estimate of coefficient	Confidence interval for coefficient		Calibration model coefficient units
					Lower 90%	Upper 90%	
Sources							
Population	0.79	0.024	0.32	0.76	0.28	1.34	$kg\cdot ps^{-1}\cdot year^{-1}$
Forest land	2.07	0.42	2.51	2.73	0	7.19	$kg\cdot ha^{-1}\cdot year^{-1}$
Environmental factors							
Precipitation	−0.033	0.21	0.026	−0.031	−0.073	0.013	cm
Carbonate area	−0.0046	0.038	0.0021	−0.0047	−0.0087	−0.0013	km^2
Aquatic loss							
Instream loss	1.95	0.053	0.96	2.15	0.41	4.04	day^{-1}
Reservoir attenuation	57.93	0.46	77.60	65.32	0	181.35	$m\cdot day^{-1}$
R^2	0.86						
RMSE	0.74						
Number of observations	29						

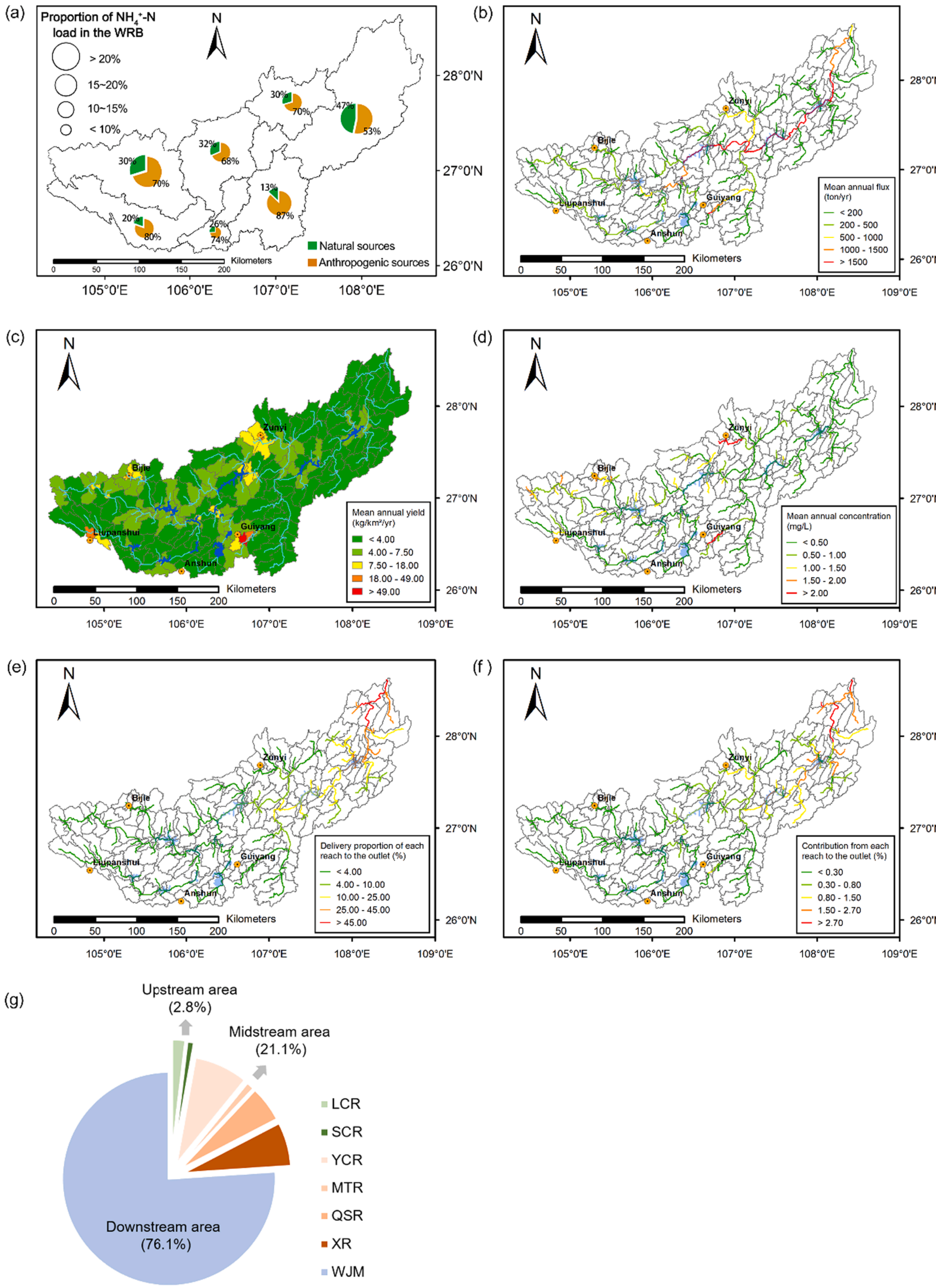

Fig. 6. The results of model prediction: (a) proportion of the NH_4^+-N from anthropogenic sources and natural sources in seven main basins of WRB; (b) the annual delivered load; (c) the annual output NH_4^+-N load per square kilometer; (d) the annual NH_4^+-N concentration; (e) the proportion of NH_4^+-N that was delivered to the outlet; (f) the contribution of each reach to the outlet and (g) the contribution from seven subbasins to the outlet.

municipal wastewater (Lang et al., 2006; Li et al., 2010).

To assess NH_4^+-N yields, the load of locally delivered NH_4^+-N per square kilometer was estimated for each of the 220 subbasins to represent the spatial variations in the NH_4^+-N yield intensity (Fig. 6c). Overall, the yield intensity tended to be higher in the upstream and midstream areas, while it was lower in the downstream area, which concurred with the distribution pattern of population (e.g., the population density decreased from southwest to northeast). Also note that the area around the cities tended to yield more NH_4^+-N, owing to the inputs from industry and municipal sewage. Hence, the results indicated that the anthropogenic NH_4^+-N sources exerted a larger impact on the NH_4^+-N transport in the WRB.

Based on the transport load and streamflow data, the three-year-averaged concentration of NH_4^+-N from 2010 to 2012 was shown in Fig. 6d. The reaches with higher NH_4^+-N concentrations were mainly located near headwater and city areas, especially around Guiyang and Zunyi with the highest values in the WRB. As for headwater reaches, higher NH_4^+-N concentrations might be caused by lower streamflow rates and thus less dilution (e.g., no upstream water input). According to the National Environmental Quality Standards for Surface Water (https://www.mee.gov.cn/), the proportion of reaches with NH_4^+-N concentrations less than that of level III (<1 mg/L) was 82.7%, 13.6% for level IV (1 to 1.5 mg/L) and V (1.5 to 2 mg/L), and the rest higher than level V (>2 mg/L). Note that among the reaches with NH_4^+-N concentrations >1 mg/L, headwaters accounted for 65.8%, which underscored the importance of headwaters in affecting the water quality of the WRB.

Fig. 6e presents the proportion of the NH_4^+-N load from the 220 reaches that was delivered to the basin outlet. With the long-distance transport and interception of the reservoirs in the upstream and midstream areas, there was a large amount of the NH_4^+-N load decayed in waterbodies and only a small portion was delivered to the outlet. By contrast, a higher proportion of the NH_4^+-N load delivered to the outlet was from the downstream area. Based on the delivery proportion map, the contributions of the NH_4^+-N load from the 220 reaches to the outlet are shown in Fig. 6f, further highlighting the importance of transport distances in affecting the NH_4^+-N transport at basin scales. Overall, 2.8% of the NH_4^+-N load delivered to the outlet was from the upstream area, 21.1% from the midstream area, and 76.1% from the downstream area (Fig. 6g).

3.3. Factors controlling NH4$^+$-N transport

3.3.1. Leakage effect in the karst area

In this study, the parameter of the carbonate area was negative in the model (Table 2), indicating that the carbonate area was negatively related to the amount of NH_4^+-N transported to streams. Part of the reason was that the groundwater systems could act as a net sink for NH_4^+-N by increasing residence times of NH_4^+-N and degrading NH_4^+-N through biogeochemical processes (Zhang et al., 2020b), and thus reduce the load from land surface to surface waterbodies. The distribution of carbonate areas is shown in Fig. 2, and the proportion of pure carbonate areas in the seven subbasins ranged from 42.7% to 61.9%. The estimation of leakage effect on the NH_4^+-N transport was based on the comparison between two scenarios as mentioned in Section 2.4.

Overall, the transport reduction in NH_4^+-N due to the leakage effect was about 36.9% for the WRB. For the seven main subbasins, the reduction rate ranged from 31.3% to 52.2%, which was generally higher in areas with larger carbonate coverage (Fig. 7). For example, the highest reduction was found in the QSR with the largest carbonate coverage. Although the carbonate coverage in the MTR was close to that for the QSR, the reduction differed noticeably between the two subbasins. Possible reasons could be attributed to: (a) the QSR was more adjacent to the Guiyang city and therefore received more anthropogenic loads that were leaked into groundwater; (b) there were two large reservoirs (i.e., HFH and BHH) located in the MTR with higher interception efficiencies for the NH_4^+-N transport (see the next section for detailed discussions), decreasing the reduction from leakage; and (c) the spatial distributions of the carbonate area and *P* intensity were different between the two subbasins, which might lead to different combined effects on surface NH_4^+-N transport as *P* could tremendously promote infiltration and leakage of NH_4^+-N to groundwater in carbonate areas. Moreover, the higher reduction rate in the XR might be also owing to its adjacency to the Zunyi city. For the other four subbasins (SCR, LCR, YCR, and WJM), the reduction rates were lower due to their relatively low carbonate coverage.

Due to the well-developed groundwater systems in the WRB, the leakage of surface water had a significant impact on the NH_4^+-N transport, which made the groundwater systems in the karst area more vulnerable to nutrient inputs and thus the deterioration of water quality (Doerfliger et al., 1999). For example, in the areas adjacent to Guiyang and Zunyi, NO_3^--N and NH_4^+-N were found in groundwater owing to human activities from fertilizer usage, and industrial and sewage wastewater discharges (Lang et al., 2006; Li et al., 2010; Liu et al., 2006).

3.3.2. Reservoir interception

Twelve reservoirs were located in the main stream and tributaries of the WRB. The reservoirs not only were important in regional water resources management, but also had large impacts on regional ecology. The parameters used in the estimation of the reservoir interception were summarized in Table 3. The definition of each parameter was given in Section 2.4.

The HJD reservoir had the largest interception load (~699 tons year^{-1}) with an interception efficiency of ~46.1%, which could be

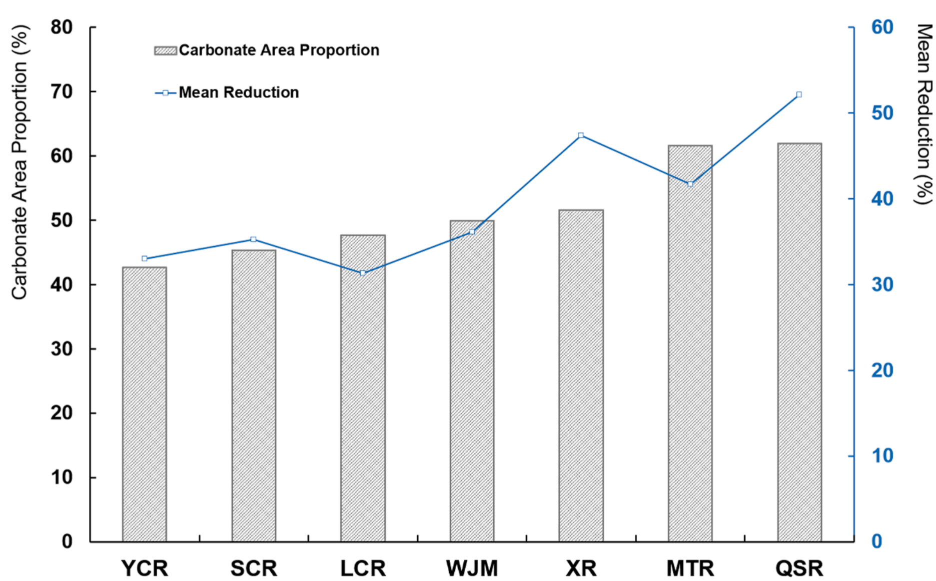

Fig. 7. The carbonate area proportion and the mean reduction for nutrient transport by leakage in seven subbasins.

Table 3
The predicted retention of NH_4^+-N in each reservoir.

Reservoir name	Water area (km^2)	Input load (tons $year^{-1}$)	Output load (tons $year^{-1}$)	Interception load (tons $year^{-1}$)	Interception efficiency (%)
HJD	41.85	1517.2	818.1	699.1	46.1
PZ	12.74	465.2	277.3	187.9	40.4
PD	11.24	632.4	472.3	160.1	25.3
YZD	7.70	438.8	365.1	73.7	16.8
DF	9.81	1340.1	1218.7	121.4	9.1
HFH	44.78	235.2	49.1	186.1	79.1
BHH	9.91	152.7	87.7	65.0	42.6
HY	1.20	358.9	338.3	20.6	5.8
SFY	3.10	1545.4	1508.0	37.4	2.4
WJD	40.35	2605.3	2077.3	528.0	20.3
GPT	31.31	2445.1	2182.3	262.8	10.7
SL	24.30	2108.6	1948.7	159.9	7.6

attributed to the following three characteristics: (a) the water depth was low, which could promote the exchange of NH_4^+-N between surface water and sediments (Wang et al., 2002); (b) the HJD reservoir resided in the upstream area, meaning relatively lower streamflow rates and thus higher residence times of NH_4^+-N in the reservoir; and (c) the water area of the HJD reservoir was relatively large (~41.85 km^2), making NH_4^+-N prone to escape via the water-atmosphere interface. These conditions are conducive to related biogeochemical processes, such as nitrification, algae absorption, and sedimentation (Zhang et al., 2009). In contrast, for the WJD reservoir with a water area of 40.35 km^2, which was located in the midstream with more input loads from upstream rivers, the interception efficiency was only ~20.3%, most likely owing to its higher streamflow rates.

The results indicated that only four reservoirs (HFH, HJD, BHH, and PZ) had the interception efficiency of >40%, while the interception efficiency of the other eight reservoirs ranged from 2.4% to 25.3%. By comparing these two groups (high efficiency group and low efficiency group as shown in Fig. 8 for a demonstration purpose), it is clear that the reservoirs of the high efficiency group were mostly located in the upstream of either the WRB or the tributaries, suggesting longer residence times of NH_4^+-N in those reservoirs for the removal of NH_4^+-N. In addition, these reservoirs generally had larger or more lake-type water areas, which were conducive to the biogeochemical processes of NH_4^+-N as explained previously (Morales-Marín et al., 2017). For the reservoirs that resembled river-type shapes (e.g., WJD), high streamflow rates most likely led to the lower interception efficiencies of NH_4^+-N. Besides their shorter residence times, the narrow shapes of those reservoirs were not conducive to the NH_4^+-N decay processes due to comparatively smaller surface water areas. In short, the results revealed that the interception efficiency of lake-type reservoirs was generally higher than that of river-type reservoirs in the WRB, which is critical for understanding the damming effect on biogeochemical processes in karst regions (Li et al., 2020).

3.4. Management strategy optimization

The SPARROW model has been extended to include a web-based decision support system for managing water quality in the contiguous U.S. (Booth et al., 2011). Based on scenario simulations (e.g., changes in land use and/or fertilizer usage amount), the model can be used to evaluate the impact of different management strategies on nutrient transport. Within the WRB, 82.7% of the reaches showed NH_4^+-N concentrations at level III (<1 mg/L); however, for the SCR, YCR, QSR, and XR subbasins, the proportion of reaches with NH_4^+-N concentrations >1 mg/L was considerably higher (37.5%, 24.1%, 25%, and 26.7%, respectively). Generally, those reaches with high NH_4^+-N concentrations were distributed in the headwater areas or the areas adjacent to cities. As for the target of >80% of reaches with the NH_4^+-N concentrations <1 mg/L (level III) in the seven subbasins, the optimized management should be focused on the SCR, YCR, QSR, and XR subbasins. Since natural inputs of NH_4^+-N were mainly from the decomposition of soil organic matter and thus difficult to be constrained, the management control was implemented by simulating different scenarios of anthropogenic inputs.

To provide useful information for watershed management and policy making, 3 scenarios, including the decreases of 10%, 20%, and 30% in anthropogenic sources, were simulated and the associated water quality

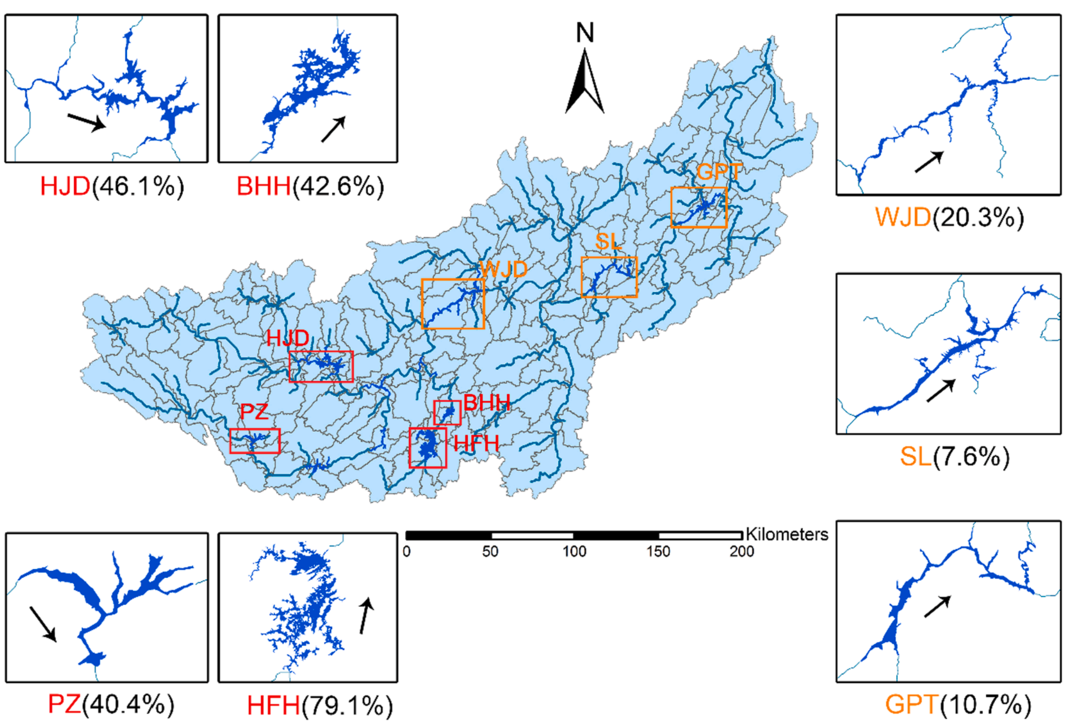

Fig. 8. The interception efficiency comparison between reservoirs of high efficiency group (>40%) and low efficiency group (<25%).

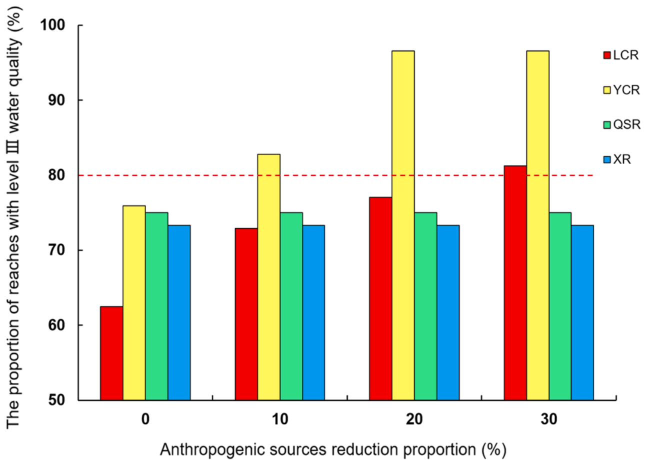

Fig. 9. The improvement of water quality in four subbasins with the reduction of anthropogenic load.

improvement is shown in Fig. 9. For LCR and YCR, when the anthropogenic inputs were decreased by 30% and 10%, respectively, the water quality control target was achieved; whereas, it failed to reach the same target in QSR and XR, even with the 30% reduction in anthropogenic inputs. The likely reason was the large amount of NH_4^+-N input to the QSR and XR reaches from the city areas. Therefore, further optimizations (e.g., moving industry to the area away from cities, or decentralizing population in urban areas) are needed for better management of NH_4^+-N to reach the set control targets for QSR and XR.

4. Conclusions

In this study, a water quality model SPARROW was constructed for the Wujiang River Basin. The model estimated the mean annual transport, concentration, and yield of NH_4^+-N from 2010 to 2012. The impacts of two important factors on NH_4^+-N transport, including the leakage effect due to the carbonate area and the interception effect from reservoirs, were analyzed. According to the model results, water quality improvement strategies were recommended. The conclusions of this study were as follows:

(1) Anthropogenic sources were the main origin of NH_4^+-N in the Wujiang River Basin. In the upstream and midstream areas, anthropogenic sources contributed >70% of NH_4^+-N to waterbodies, while the contributions from anthropogenic and natural sources were equally important in the downstream area.
(2) The leakage of surface water could make reduction in the transport of NH_4^+-N for about 36.9% with a range from 31.3% to 52.2% in the seven main subbasins. Generally, the leakage effect was more significant in subbasins with higher carbonate area coverage.
(3) The interception efficiency differed among the 12 reservoirs in the Wujiang River Basin. The flow rate and water area of reservoirs were the primary factors affecting the interception efficiency.
(4) As for the target of >80% reaches to reach water quality of level III, the Sancha River and Yachi River subbasins needed a reduction of 30% and 10% in NH_4^+-N from anthropogenic sources, respectively. However, for the Xiang River and Qingshui River subbasins, a further reduction was required to reach the target of 80%.

CRediT authorship contribution statement

Yibin Dai: Conceptualization, Methodology, Writing - original draft. **Yunchao Lang:** Resources, Supervision, Writing - review & editing. **Tiejun Wang:** Investigation, Project administration, Writing - review & editing. **Xiaokun Han:** Writing - review & editing. **Lichun Wang:** Writing - review & editing. **Jun Zhong:** Writing - review & editing.

Declaration of competing interest

The authors declare that they have no known competing financial interests or personal relationships that could have appeared to influence the work reported in this paper.

Acknowledgments

This study was supported by the National Key Research and Development Program of China (Grant No. 2016YFA0601002), the National Natural Science Foundation of China (Grant No. U1612441) and the Strategic Priority Research Program of Chinese Academy of Sciences (Grant No. XDB40000000). The authors would also like to acknowledge the financial support from the Tianjin University for this study.

Appendix A. Supplementary data

Supplementary data to this article can be found online at https://doi.org/10.1016/j.jhydrol.2020.125763.

References

Abbaspour, K.C., Yang, J., Maximov, I., Siber, R., Bogner, K., Mieleitner, J., Zobrist, J., Srinivasan, R., 2007. Modelling hydrology and water quality in the pre-alpine/alpine Thur watershed using SWAT. J. Hydrol. 333, 413–430. https://doi.org/10.1016/j.jhydrol.2006.09.014.

Aguilera, R., Marcé, R., Sabater, S., 2012. Linking in-stream nutrient flux to land use and inter-annual hydrological variability at the watershed scale. Sci. Total Environ. 440, 72–81. https://doi.org/10.1016/j.scitotenv.2012.08.030.

Alexander, R.B., Smith, R.A., Schwarz, G.E., 2000. Effect of stream channel size on the delivery of nitrogen to the Gulf of Mexico. Nature 403, 758–761.

Alexander, R.B., Elliott, A.H., Shankar, U., McBride, G.B., 2002. Estimating the sources and transport of nutrients in the Waikato River Basin, New Zealand. Water Resour. Res. 38, 4–1–4–23. https://doi.org/10.1029/2001WR000878.

Alexander, R.B., Smith, R.A., Schwarz, G.E., Boyer, E.W., Nolan, J.V., Brakebill, J.W., 2007. Differences in phosphorus and nitrogen delivery to the Gulf of Mexico from the Mississippi River Basin. Environ. Sci. Technol. 42, 822–830. https://doi.org/10.1021/es0716103.

Alshawaf, M., Douglas, E., Ricciardi, K., 2016. Estimating nitrogen load resulting from biofuel mandates. Int. J. Environ. Res. Public Health 13, 478. https://doi.org/10.3390/ijerph13050478.

Amin, M.G.M., Veith, T.L., Collick, A.S., Karsten, H.D., Buda, A.R., 2016. Simulating hydrological and nonpoint source pollution processes in a karst watershed: a variable source area hydrology model evaluation. Agric. Water Manag. 180, 212–223. https://doi.org/10.1016/j.agwat.2016.07.011.

Booth, N.L., Everman, E.J., Kuo, I.L., Sprague, L., Murphy, L., 2011. A web-based decision support system for assessing regional water-quality conditions and management actions. J. Am. Water Resour. Assoc. 47, 1136–1150. https://doi.org/10.1111/j.1752-1688.2011.00573.x.

Brown, J.B., Sprague, L.A., Dupree, J.A., 2011. Nutrient sources and transport in the Missouri River Basin, with emphasis on the effects of irrigation and reservoirs. J. Am. Water Resour. Assoc. 47, 1034–1060. https://doi.org/10.1111/j.1752-1688.2011.00584.x.

Čerkasova, N., Umgiesser, G., Ertürk, A., 2018. Development of a hydrology and water quality model for a large transboundary river watershed to investigate the impacts of climate change – a SWAT application. Ecol. Eng. 2018 (124), 99–115. https://doi.org/10.1016/j.ecoleng.2018.09.025.

Chen, Y., Xu, C.Y., Chen, X., Xu, Y., Yin, Y., Gao, L., Liu, M., 2019. Uncertainty in simulation of land-use change impacts on catchment runoff with multi-timescales based on the comparison of the HSPF and SWAT models. J. Hydrol. 573, 486–500.

Doerfliger, N., Jeannin, P.Y., Zwahlen, F., 1999. Water vulnerability assessment in karst environments: a new method of defining protection areas using a multi-attribute approach and GIS tools (EPIK method). Environ. Geol. 39, 165–176.

Duan, W.L., He, B., Takara, K., Luo, P.P., Nover, D., Hu, M.C., 2015. Modeling suspended sediment sources and transport in the Ishikari River basin, Japan, using SPARROW. Hydrol. Earth Syst. Sci. 19, 1293–1306. https://doi.org/10.5194/hess-19-1293-2015.

Feng, X., Jiang, H., Qiu, G., Yan, H., Li, G., Li, Z., 2009. Geochemical processes of mercury in Wujiangdu and Dongfeng reservoirs, Guizhou. China. Environ. Pollut. 157, 2970–2984. https://doi.org/10.1016/j.envpol.2009.06.002.

Fowler, D., Coyle, M., Skiba, U., Sutton, M.A., Cape, J.N., Reis, S., Sheppard, L.J., Jenkins, A., Grizzetti, B., Galloway, J.N., Vitousek, P., Leach, A., Bouwman, A.F., Butterbach-Bahl, K., Dentener, F., Stevenson, D., Amann, M., Voss, M., 2013. The global nitrogen cycle in the twenty-first century. Phil. Trans. R. Soc. 368, 20130164. https://doi.org/10.1098/rstb.2013.0164.

Garcia, A.M., Hoos, A.B., Terziotti, S., 2011. A regional modeling framework of phosphorus sources and transport in streams of the Southeastern United States. J. Am. Water Resour. Assoc. 47, 991–1010. https://doi.org/10.1111/j.1752-1688.2010.00517.x.

Han, G., Li, F., Tan, Q., 2014. Effects of land use on water chemistry in a river draining karst terrain, southwest China. Hydrol. Sci. J. 59, 1063–1073. https://doi.org/10.1080/02626667.2014.902948.

Harrison, J.A., Maranger, R.J., Alexander, R.B., Giblin, A.E., Jacinthe, P.A., Mayorga, E., Seitzinger, S.P., Sobota, D.J., Wollheim, W.M., 2009. The regional and global significance of nitrogen removal in lakes and reservoirs. Biogeochemistry 93, 143–157. https://doi.org/10.1007/s10533-008-9272-x.

Hartmann, A., Goldscheider, N., Wagener, T., Lange, J., Weiler, M., 2014. Karst water resources in a changing world: review of hydrological modeling approaches. Rev. Geophys. 52, 218–242. https://doi.org/10.1002/2013RG000443.

Hashemi, F., Olesen, J.E., Dalgaard, T., Børgesen, C.D., 2016. Review of scenario analyses to reduce agricultural nitrogen and phosphorus loading to the aquatic environment. Sci. Total Environ. 573, 608–626. https://doi.org/10.1016/j.scitotenv.2016.08.141.

Huang, Q.B., Qin, X.Q., Liu, P.Y., Zhang, L.K., Su, C.T., 2017. Impact of sulfuric and nitric acids on carbonate dissolution, and the associated deficit of CO_2 uptake in the upper–middle reaches of the Wujiang River. China. J. Contam. Hydrol. 203, 18–27. https://doi.org/10.1016/j.jconhyd.2017.05.006.

Jiang, Z., Lian, Y., Qin, X., 2014. Rocky desertification in Southwest China: impacts, causes, and restoration. Earth-Science Rev. 132, 1–12. https://doi.org/10.1016/j.earscirev.2014.01.005.

Kalhor, K., Ghasemizadeh, R., Rajic, L., Alshawabkeh, A., 2019. Assessment of groundwater quality and remediation in karst aquifers: a review. Groundw. Sustain. Dev. 8, 104–121. https://doi.org/10.1016/j.gsd.2018.10.004.

Kyllmar, K., Carlsson, C., Gustafson, A., Ulén, B., Johnsson, H., 2006. Nutrient discharge from small agricultural catchments in Sweden: characterisation and trends. Agric. Ecosyst. Environ. 115, 15–26. https://doi.org/10.1016/j.agee.2005.12.004.

Lang, Y.C., Liu, C.Q., Zhao, Z.Q., Li, S.L., Han, G.L., 2006. Geochemistry of surface and ground water in Guiyang. China: water/rock interaction and pollution in a karst hydrological system. Appl. Geochemistry 21, 887–903. https://doi.org/10.1016/j.apgeochem.2006.03.005.

Lauber, U., Goldscheider, N., 2014. Use of artificial and natural tracers to assess groundwater transit-time distribution and flow systems in a high-alpine karst system (Wetterstein Mountains, Germany). Hydrogeol. J. 22, 1807–1824. https://doi.org/10.1007/s10040-014-1173-6.

Li, C., Ji, H., 2016. Chemical weathering and the role of sulfuric and nitric acids in carbonate weathering: isotopes (^{13}C, ^{15}N, ^{34}S, and ^{18}O) and chemical constraints. J. Geophys. Res. Biogeosci. 121, 1288–1305.

Li, S.L., Liu, C.Q., Lang, Y.C., Zhao, Z.Q., Zhou, Z.H., 2010. Tracing the sources of nitrate in karstic groundwater in Zunyi. Southwest China: a combined nitrogen isotope and water chemistry approach. Environ. Earth Sci. 60, 1415–1423. https://doi.org/10.1007/s12665-009-0277-0.

Li, S.L., Liu, C.Q., Li, J., Xue, Z., Guan, J., Lang, Y., Ding, H., Li, L., 2013. Evaluation of nitrate source in surface water of southwestern China based on stable isotopes. Environ. Earth Sci. 68, 219–228.

Li, X., Wellen, C., Liu, G., Wang, Y., Wang, Z.L., 2015. Estimation of nutrient sources and transport using Spatially Referenced Regressions on Watershed Attributes: a case study in Songhuajiang River Basin. China. Environ. Sci. Pollut. Res. 22, 6989–7001. https://doi.org/10.1007/s11356-014-3903-7.

Li, Z., Xu, X., Yu, B., Xu, C., Liu, M., Wang, K., 2016. Quantifying the impacts of climate and human activities on water and sediment discharge in a karst region of southwest China. J. Hydrol. 542, 836–849. https://doi.org/10.1016/j.jhydrol.2016.09.049.

Li, S.L., Xu, S., Wang, T.J., Yue, F.J., Peng, T., Zhong, J., Wang, L.C., Chen, J.A., Wang, S. J., Chen, X., Liu, C.Q., 2020. Effects of agricultural activities coupled with karst structures on riverine biogeochemical cycles and environmental quality in the karst region. Agric. Ecosyst. Environ. 303, 107120. https://doi.org/10.1016/j.agee.2020.107120.

Liu, C.Q., Li, S.L., Lang, Y.C., Xiao, H.Y., 2006. Using $\delta^{15}N$- and $\delta^{18}O$-values to identify nitrate sources in karst ground water, Guiyang, southwest China. Environ. Sci. Technol. 40, 6928–6933. https://doi.org/10.1021/es0610129.

Liu, X.L., Liu, C.Q., Li, S.L., Wang, F.S., Wang, B.L., Wang, Z.L., 2011. Spatiotemporal variations of nitrous oxide (N_2O) emissions from two reservoirs in SW China. Atmos. Environ. 45, 5458–5468. https://doi.org/10.1016/j.atmosenv.2011.06.074.

Malagò, A., Efstathiou, D., Bouraoui, F., Nikolaidis, N.P., Franchini, M., Bidoglio, G., Kritsotakis, M., 2016. Regional scale hydrologic modeling of a karst-dominant geomorphology: the case study of the Island of Crete. J. Hydrol. 540, 64–81. https://doi.org/10.1016/j.jhydrol.2016.05.061.

McMahon, G., Alexander, R.B., Qian, S., 2003. Support of TMDL programs using spatially referenced regression models. J. Water Resour. Plan. Manag. 129, 315–329.

Morales-Marín, L.A., Wheater, H.S., Lindenschmidt, K.E., 2017. Assessment of nutrient loadings of a large multipurpose prairie reservoir. J. Hydrol. 550, 166–185. https://doi.org/10.1016/j.jhydrol.2017.04.043.

Peng, X., Dai, Q., Ding, G., Li, C., 2019. Role of underground leakage in soil, water and nutrient loss from a rock-mantled slope in the karst rocky desertification area. J. Hydrol. 578, 124086. https://doi.org/10.1016/j.jhydrol.2019.124086.

Perrin, J.L., Raïs, N., Chahinian, N., Moulin, P., Ijjaali, M., 2014. Water quality assessment of highly polluted rivers in a semi-arid Mediterranean zone Oued Fez and Sebou River (Morocco). J. Hydrol. 510, 26–34. https://doi.org/10.1016/j.jhydrol.2013.12.002.

Peterson, B.J., Wollheim, W.M., Mulholland, P.J., Webster, J.R., Meyer, J.L., Tank, J.L., Marti, E., Bowden, W.B., Valett, H.M., 2001. Control of nitrogen export from watersheds by headwater streams. Science 292, 86–90. https://doi.org/10.1126/science.1056874.

Qin, B., Zhu, G., Gao, G., Zhang, Y., Li, W., Paerl, H.W., Carmichael, W.W., 2010. A drinking water crisis in Lake Taihu, China: linkage to climatic variability and lake management. Environ. Manag. 45, 105–112. https://doi.org/10.1007/s00267-009-9393-6.

Robertson, D.M., Saad, D.A., 2011. Nutrient inputs to the Laurentian Great Lakes by source and watershed estimated using sparrow watershed models. J. Am. Water Resour. Assoc. 47, 1011–1033. https://doi.org/10.1111/j.1752-1688.2011.00574.x.

Schulze, K., Hunger, M., Döll, P., 2005. Simulating river flow velocity on global scale. Adv. Geosci. 5, 133–136. https://doi.org/10.5194/adgeo-5-133-2005.

Schwarz, G.E., Hoos, A.B., Alexander, R.B., Smith, R.A., 2006. The SPARROW surface water-quality model: theory, application and user documentation. U.S. Geol. Surv. Tech. Methods Report, Reston, U.S., pp. 1–78

Seitzinger, S.P., Styles, R.V., Boyer, E.W., Alexander, R.B., Billen, G., Howarth, R.W., Mayer, B., Van Breemen, N., 2002. Nitrogen retention in rivers: model development and application to watersheds in the northeastern U.S.A. Biogeochemistry 57-58, 199–237. https://doi.org/10.1023/A:1015745629794.

Singh, J., Knapp, H.V., Arnold, J.G., Demissie, M., 2005. Hydrological modeling of the Iroquois river watershed using HSPF and SWAT. J. Am. Water Resour. Assoc. 41, 343–360.

Smith, R.A., Schwarz, G.E., Alexander, R.B., 1997. Regional interpretation of water-quality monitoring data. Water Resour. Res. 33, 2781–2798. https://doi.org/10.1029/97WR02171.

Song, X., Gao, Y., Green, S.M., Wen, X., Dungait, J.A., Xiong, B., Quine, T.A., He, N., 2019. Rainfall driven transport of carbon and nitrogen along karst slopes and associative interaction characteristic. J. Hydrol. 573, 246–254. https://doi.org/10.1016/j.jhydrol.2019.03.083.

Tooth, A.F., Fairchild, I.J., 2003. Soil and karst aquifer hydrological controls on the geochemical evolution of speleothem-forming drip waters, Crag Cave, southwest Ireland. J. Hydrol. 273, 51–68.

Wang, Y., Wan, G., Huang, R., Huang, R., 2002. Distribution of total, exchangeable and fixed nitrogen in the sediments of two lakes in Guizhou Province. J. Lake Sci. 14, 301–309 (in Chinese).

Wang, F., Yu, Y., Liu, C., Wang, B., Wang, Y., Guan, J., 2010. Dissolved silicate retention and transport in cascade reservoirs in Karst area. Southwest China. Sci. Total Environ. 408, 1667–1675. https://doi.org/10.1016/j.scitotenv.2010.01.017.

Wang, W., Li, S.L., Zhong, J., Li, C., Yi, Y., Chen, S., Ren, Y., 2019a. Understanding transport and transformation of dissolved inorganic carbon (DIC) in the reservoir system using δ^{13}CDIC and water chemistry. J. Hydrol. 574, 193–201. https://doi.org/10.1016/j.jhydrol.2019.04.036.

Wang, B., Zhang, H., Liang, X., Li, X., Wang, F., 2019b. Cumulative effects of cascade dams on river water cycle: evidence from hydrogen and oxygen isotopes. J. Hydrol. 568, 604–610. https://doi.org/10.1016/j.jhydrol.2018.11.016.

Wei, X., Xie, S., Zhang, Z., Chen, Z., 2011. Characteristics of surface soil erosion of karst valley in different land use types at Nanping in Chongqing. Trans. Chin. Soc. Agric. Eng. 27, 42–46 (doi:1002-6819(2011)-06-0042-05, in Chinese).

Wellen, C., Arhonditsis, G. B., Labencki, T., Boyd, D., 2012. A Bayesian methodological framework for accommodating interannual variability of nutrient loading with the SPARROW model. Water Res. Res. 48, 1–22. doi:https://doi.org/10.1029/2012WR011821, 2012.

Xia, X., Zhang, S., L., S., Zhang, L., Wang, G., Zhang, L., Wang, J., Li, Z., 2018. The cycle of nitrogen in river systems: sources, transformation, and flux. Environ. Sci. Processes Impacts 20, 863–891.

Yuan, D.X., 1997. Rock desertification in the subtropical karst of south China. Geomorphol. 108, 81–90.

Zhang, L., Hickel, K., Dawes, W.R., Chiew, F.H., Western, A.W., Briggs, P.R., 2004. A rational function approach for estimating mean annual evapotranspiration. Water Resour. Res. 40, 1–14. https://doi.org/10.1029/2003WR002710.

Zhang, C.P., Liu, C.Q., Wu, P., Wang, F.S., Wang, B.L., 2009. Distribution characteristics of N, Si in middle and upper reaches of Wujiang River in summer-autumn season. Resour. Environ. Yangtze Basin 18, 331–336 (doi:1004-8227(2009)04-0331-06, in Chinese).

Zhang, L., Chen, Y., Zhao, Y., Henze, D.K., Zhu, L., Song, Y., Paulot, F., Liu, X., Pan, Y., Lin, Y., Huang, B., 2018a. Agricultural ammonia emissions in China: reconciling bottom-up and top-down estimates. Atmos. Chem. Phys. 18, 339–355. https://doi.org/10.5194/acp-18-339-2018.

Zhang, Y., Schaap, M.G., Zha, Y., 2018b. A high-resolution global map of soil hydraulic properties produced by a hierarchical parameterization of a physically-based water retention model. Water Resour. Res. 54, 9774–9790. https://doi.org/10.1029/2018WR023539.

Zhang, Z., Chen, X., Cheng, Q., Soulsby, C., 2020a. Characterising the variability of transit time distributions and young water fractions in karst catchments using flux tracking. Hydrol. Process. 34, 3156–3174. https://doi.org/10.1002/hyp.13829.

Zhang, Z., Chen, X., Cheng, Q., Li, S., Yue, F., Peng, T., Waldron, S., Oliver, D.M., Soulsby, C., 2020b. Coupled hydrological and biogeochemical modelling of nitrogen transport in the karst critical zone. Sci. Total Environ. 732, 138902.

Zhou, P., Huang, J., Hong, H., 2018. Modeling nutrient sources, transport and management strategies in a coastal watershed. Southeast China. Sci. Total Environ. 610-611, 1298–1309. https://doi.org/10.1016/j.scitotenv.2017.08.113.